

1       **An integrated dataset of ground hydrothermal regimes and soil**  
2       **nutrients monitored during 2016-2022 in some previously burned**  
3       **areas in hemiboreal forests in Northeast China**

4       Xiaoying Li <sup>1</sup>, Huijun Jin <sup>1,2,3,\*</sup>, Qi Feng <sup>4</sup>, Qingbai Wu <sup>1</sup>, Hongwei Wang <sup>1,2</sup>, Ruixia He <sup>1</sup>,  
5       Dongliang Luo <sup>1</sup>, Xiaoli Chang <sup>1,5</sup>, Raul-David Şerban <sup>6</sup>, and Tao Zhan <sup>3</sup>

6       <sup>1</sup> Key Laboratory of Cryospheric Science and Frozen Soil Engineering, Northwest Institute of Eco-Environment  
7       and Resources, Chinese Academy of Sciences, Lanzhou 730000, China;

8       <sup>2</sup> School of Ecology, School of Civil Engineering and Transportation, China-Russia Joint Laboratory of Cold  
9       Regions Engineering and Environment, and Permafrost Institute, Northeast Forestry University, Harbin  
10       150040, China;

11       <sup>3</sup> Ministry of Natural Resources Field Observation and Research Station of Permafrost and Cold Regions  
12       Environment in the Da Xing'anling Mountains at Mo'he, Natural Resources Survey Institute of Heilongjiang  
13       Province, Harbin 150036, China;

14       <sup>4</sup> Key Laboratory of Ecohydrology of Inland River Basin, Northwest Institute of Eco-Environment and Resources,  
15       Chinese Academy of Sciences, Lanzhou 730000, China;

16       <sup>5</sup> Hunan University of Science and Technology, Xiangtan, Hunan 411202, China and;

17       <sup>6</sup> Faculty of Agricultural, Environmental and Food Sciences, Free University of Bozen-Bolzano, Bolzano 39100,  
18       Italy

19       \* Corresponding authors: Huijun Jin ([hjjin@nefu.edu.cn](mailto:hjjin@nefu.edu.cn)) at the School of Civil Engineering and Transportation,  
20       Northeast Forestry University, Harbin 150040, China

21       **Abstract:**

22       Under a warming climate, occurrences of wildfires have been increasingly more  
23       frequent in boreal forests and arctic tundra during the last few decades. Wildfires can  
24       cause radical changes in the forest ecosystems and permafrost environment, such as  
25       irreversible degradation of permafrost, succession of boreal forests, rapid and massive

26 losses of soil carbon stock, and increased periglacial geohazards. Since 2016, we have  
27 gradually and more systematically established a network for studying soil nutrients and  
28 monitoring the hydrothermal state of the active layer and near-surface permafrost in the  
29 northern Da Xing'anling (Hinggan) Mountains in Northeast China. The datasets of soil  
30 moisture content (0-9.4 m in depth), soil organic carbon (0-3.6 m), total nitrogen (0-3.6  
31 m), and total phosphorus and potassium (0-3.6 m) were obtained by field sampling and  
32 ensuing laboratory tests in 2016. The datasets of ground temperatures (0-20 m) and  
33 active layer thickness (2017-2022) were obtained by thermistor cables permanently  
34 installed in boreholes or interpolated with these temperatures. The present data can be  
35 used to simulate changes in permafrost features under a changing climate and wildfire  
36 disturbances and to explore the changing interactive mechanisms of the fire-permafrost-  
37 carbon system in the hemiboreal forest. Furthermore, they can provide baseline data for  
38 studies and action plans to support the carbon neutralization initiative and assessment  
39 of ecological safety and management of the permafrost environment. These datasets  
40 can be easily accessed from the National Tibetan Plateau/Third Pole Environment Data  
41 Center (<https://doi.org/10.11888/Cryos.tpcdc.300933>, Li and Jin, 2024).

## 42 **1 Introduction**

43 As a key component of the Northern Hemisphere, permafrost and its changes can  
44 have substantial consequences for natural and man-made systems (Smith et al., 2022).  
45 Moreover, due to its high sensitivity to climate warming, surface disturbances, and  
46 human activities, permafrost has undergone extensive degradation during the last six  
47 decades (e.g., Biskaborn et al., 2019; Chang et al., 2024; Jin et al., 2000, 2007, 2021,  
48 2022, 2023; Li et al., 2022a; Petrov et al., 2022). As one of the most common natural  
49 agents and disturbance factors in boreal forests, wildfires can initiate ecosystem  
50 renewal at different spatiotemporal scales (Johnstone et al., 2004; Li et al., 2019).  
51 Wildfires impact the permafrost environment first by modifying or altering the ground  
52 hydrothermal regimes (Jorgenson et al., 2013; Li et al., 2022b; Yoshikawa et al., 2003),  
53 and subsequently by inducing modifications or radical/irreversible changes in

54 biogeochemical processes (e.g., Fultz et al., 2016; Li et al., 2023; Ping et al., 2010; Xu  
55 et al., 2024). In boreal forests, wildfires have become increasingly more frequent in  
56 recent decades under a warming climate and increasing human activities (Boyd et al.,  
57 2023; Chen et al., 2023; Knorr et al., 2016; Westerling et al., 2006). Moreover, the  
58 region immediately south of the Arctic circle (50°N-67°N) experienced a greater  
59 number of vegetation fires compared to the Arctic (north of 67°N) in 2001-2020 (Chen  
60 et al., 2023). Although the total burned area on Earth may be declining, the fire behavior  
61 was worsening in several regions in 2003–2023, particularly the boreal and temperate  
62 conifer biome (Cunningham et al., 2024).

63 In boreal regions, vegetation and soil organic layer are essential buffering and  
64 protective layers of the underlying permafrost. The combustion of all vegetation cover  
65 and partial or complete removal of the insulating organic layer have direct hydrothermal  
66 impacts on permafrost. It reduces the land surface albedo, increases ground surface and  
67 cryosol/ice exposure to direct solar radiation, and weakens the cooling effects of  
68 vegetative shading and evapotranspiration (Johnstone et al., 2010; Nossov et al., 2013;  
69 Shur and Jorgenson, 2007; Yoshikawa et al., 2003). All of these contribute to higher  
70 ground surface temperature and more heat transferred into the ground, resulting in a  
71 rapid ground warming and sharp deepening of the active layer (Li et al., 2022b;  
72 Michaelides et al., 2019; Nossov et al., 2013; Smith et al., 2015). In Interior Alaska,  
73 organic layer thickness decreased from 21 to 4 cm after fire, resulting in thaw depth  
74 increasing from 72 to 152 cm, mean annual surface temperature rising from  $-0.6$  to  
75  $+2.1^{\circ}\text{C}$  and mean annual deep temperature going up from  $-1.7$  to  $+0.4^{\circ}\text{C}$  (Nossov et  
76 al., 2013). In the boreal zone, 6-11 years after fire, mean annual ground temperature  
77 (MAGT) increased by  $1.5$ - $2.3^{\circ}\text{C}$  (Li et al., 2021; Munkhjargal et al., 2020; Nossov et  
78 al., 2013; Smith et al., 2015), even mean annual ground surface temperatures in burned  
79 areas were still  $2$ - $3^{\circ}\text{C}$  higher than those in unburned areas 80 years after fire (Brown et  
80 al., 2015). Meanwhile, 25 years after fire, the active layer thickness (ALT) could  
81 increase by  $2.75$  m, from the initial value of  $45$  cm, and ALT could not recover to the  
82 pre-fire level even 36 years after fire (Viereck et al., 2008). In Central Siberia, it

83 generally takes 70-80 years for the active layer to return to the pre-fire state (Kirdeyanov  
84 et al., 2020). Forest fires also can cause significant changes in soil moisture contents,  
85 which in turn affects ground thermal regimes (Nossov et al., 2013). Due to the fire-  
86 induced thaw of permafrost, the charred moss layers with lowered infiltration rates,  
87 lower transpiration rate and reduced evapotranspiration in severely burned areas,  
88 surface soil moisture contents (generally less than 30 cm in depth) at burned sites were  
89 significantly higher than those at unburned sites (Kopp et al., 2014; Potter and Hugny,  
90 2020; Yoshikawa et al., 2003). However, affected by soil texture, permafrost thaw after  
91 fire can also lead to a decrease in soil moisture contents (Li et al., 2022b; Nossov et al.,  
92 2013). In summary, in a short term, forest fires will decrease rates of transpiration,  
93 raising soil moisture contents; in a long-term (more than a decade), the increased ALT  
94 and recovery of vegetation will reduce soil moisture content at burned sites as compared  
95 to that at unburned sites (Yoshikawa et al., 2003). Moreover, changes in ground  
96 hydrothermal regimes and ALT would decline and progressively dwindle with  
97 ecosystem recovery and organic layer regrowth over time under a stable or cooling  
98 climate (e.g. Holloway et al., 2020; Rocha et al., 2012).

99 Arctic-boreal permafrost soils contain between 1100-1500 Pg (1 Pg=10<sup>15</sup> g)  
100 carbon, approximately twice of the carbon pool in the atmosphere (Hugelius et al.,  
101 2014), and accounting for nearly half of the global belowground organic carbon pool  
102 (O'Donnell et al., 2011a). Wildfire disturbances have important and long-term  
103 ramifications for terrestrial carbon cycling and carbon stocks (Chen et al., 2022;  
104 Dieleman et al., 2022; Genet et al., 2013; O'Donnell et al., 2011a, 2011b). Unlike  
105 gradual thawing, abrupt changes after fires in ground hydrothermal regimes often  
106 disrupt the entire soil profile and initiate or aggravate carbon loss from deep permafrost  
107 soils (Jones et al., 2015; Turetsky et al., 2019). Therefore, the combustion of vegetation  
108 and the subsequent thaw of permafrost have resulted in rapid releases of large amounts  
109 of carbon and nitrogen into the atmosphere as greenhouse gases (Mack et al., 2011,  
110 2021; Taş et al., 2014). Furthermore, over a short time, abrupt permafrost thaw would  
111 possibly result in emitting more methane than gradual thaw (Koven et al., 2015).

112 Therefore, in the boreal permafrost region, wildfire exacerbate rates of permafrost thaw  
113 and alter soil organic carbon dynamics in both organic and mineral soils. In addition to  
114 soil organic carbon, forest fires potentially also reduce soil nitrogen contents, inducing  
115 shifts in nutrient cycling in the boreal forest and permafrost regions (Certini, 2005;  
116 Knicker, 2007; Kolka et al., 2017). However, there are inconsistent reports on the  
117 effects of forest fire on soil phosphorus and potassium. Some studies show a significant  
118 post-fire reduction in phosphorus and potassium while other studies indicate an evident  
119 increase after light burns, but a reduction after severe burns, and nearly unchanged  
120 stocks of potassium and phosphorus (Gu et al., 2010; Neff et al., 2005; Zhao et al.,  
121 1994). As a result, wildfires in boreal permafrost regions had been considered to trigger  
122 strong positive feedbacks on climate warming *via* massive emissions of biogenic major  
123 greenhouse gases (Koven et al., 2015; Ramm et al., 2023).

124 Located on the southern margin of Eastern Asian boreal forests and permafrost  
125 regions, the Da Xing'anling (Hinggan) Mountains in Northeast China are prone to  
126 frequent and massive wildfires. The Xing'an permafrost here is controlled or strongly  
127 affected by many local factors, such as dense vegetation cover, thick organic layer,  
128 stable snow cover, and anthropic development (Jin et al., 2007; Şerban et al., 2021;  
129 Wang et al., 2024). The warm and thin permafrost in the Da Xing'anling Mountains in  
130 Northeast China is located in the discontinuous permafrost zone. Therefore, this  
131 ecosystem-dominated (driven, modified, or protected) permafrost is sensitive to climate  
132 warming and wildfires (Shur and Jorgenson, 2007). Compared with the Arctic  
133 permafrost region, the permafrost monitoring network in this region has been  
134 established only recently, with inadequately readily accessible and shared permafrost  
135 data. Similarly, the permafrost monitoring data in the burned areas in the boreal  
136 permafrost region in China are meagre in comparison with those other northern  
137 countries or regions, but they are increasing. Prior to the early 1980s, there was little  
138 research on wildfire impacts on the permafrost environment in Northeast China. There  
139 were only a few occasional fire-related geocryological studies in the early 1990s and  
140 limited site-specific measurements of soil temperature and moisture content in the

141 active layer and near-surface ( $\leq 20$  m in depth) permafrost near the Amu'er town,  
142 northern Heilongjiang Province (Liang et al., 1991; Zhou et al., 1993). Moreover,  
143 research on fire impacts on soil carbon and nitrogen pools and cycles in the Xing'an  
144 permafrost in Northeast China has just started and is still at its fledgling stage. Due to  
145 the cold and arid climate in winter and spring, complex mountain topography, and dense  
146 hemiboreal vegetation in the region, fire regimes are often complex. In addition, burned  
147 areas are often located in pristine forest areas far away from roads, making it  
148 challenging to timely and/or readily access and study fire impacts. Therefore, it is  
149 difficult to systematically understand and quantitatively evaluate the effects of wildfires  
150 on ground hydrothermal regimes and carbon stocks at different spatiotemporal scales  
151 (Li et al., 2021).

152 To address the abovementioned issues, since 2016, an observation system has been  
153 gradually established for ground hydrothermal regimes and soil nutrient contents in the  
154 northern Da Xing'anling Mountains. This dataset can provide important supportive data  
155 for studying permafrost landscapes, carbon stocks, and boreal ecology and hydrology.  
156 It can also provide important references for the management of land and water resources  
157 and ecological environment after wildfire disturbances in Northeast China, particularly  
158 in forested hemiboreal permafrost regions. In Section 2 of this paper, we first introduce  
159 the comprehensive observation network of permafrost and soil nutrients in the northern  
160 Da Xing'anling Mountains. The design of the monitoring network of ground  
161 hydrothermal regimes and systematic observations of soil nutrient contents, and  
162 evaluation of data quality are given in Section 2. In Section 3, observations of  
163 permafrost hydrothermal regimes and soil nutrients that provide a 6-year-long dataset  
164 are described and briefly interpreted with a focus on major features of the observation  
165 network for better understanding of the dataset structure and contents. The data  
166 availability and accessibility are provided in Section 4, and; **in Section 5, major**  
167 **conclusions and prospects are given.** This dataset provides important input for the  
168 model simulations of permafrost changes under fire disturbances and a warming climate,  
169 especially those rapid and abrupt degradation of the Xing'an permafrost and resultant

170 periglacial phenomena, such as thermokarst, thaw settlement, and ground surface  
171 subsidence and ponding. It is useful for analyzing the interactive hydrothermal and  
172 cyclic mechanisms of the wildfires-permafrost-carbon system in the hemiboreal forest.

## 173 **2 Monitoring networks and data processing**

### 174 **2.1 Study area descriptions and monitoring networks**

175 A permafrost monitoring network has been established in four burned areas in the  
176 northern Da Xing'anling Mountains in Northeast China in boreal forest and  
177 discontinuous permafrost regions (Figure 1). Two are located in shrub wetlands in  
178 Mo'he city (MH) and Gulian town (GL) in northern Heilongjiang Province. The other  
179 two are located in larch forests in Alongshan (AL) and Mangui (MG) towns in the  
180 northeastern part of Inner Mongolia. The network includes eight sites in the four burned  
181 areas with two fire severity (severely burned (S) and unburned (U)) from 1987 to 2015  
182 (the fire severity division method was shown in "2.2 *Fire severity*" section). The studied  
183 forest fire in MH (with severely burned (MH-S) and unburned (MH-U) sites) occurred  
184 on 6 May 1987, with a burned-over area of  $1.01 \times 10^6$  ha; that in GL (with severely  
185 burned (GL-S)) and unburned (GL-U) sites), on 28 July 2002, 1,121 ha; AL (with  
186 severely burned (AL-S) and unburned (AL-U) sites), on 10 May 2009, 930 ha, and; MG  
187 (with severely burned (MG-S) and unburned (MG-U) sites), on 12 July 2015, 237 ha.





204 of rain from June to August, accounting for 62%-65% of the annual total. Snow cover  
 205 generally lasted from October to the next May, with maximum snow depths at 40-50  
 206 cm.

207 The four study areas were selected to observe post-fire changes in permafrost  
 208 features and soil nutrient conditions (Table 1). This monitoring network includes eight  
 209 boreholes and soil profiles, and major elements of the observational network for ground  
 210 temperature, ALT, soil moisture content (SMC), soil organic carbon (SOC), total  
 211 nitrogen (TN), total phosphorus (TP), and total potassium (TK). The MAGT at the  
 212 depth of zero annual amplitude ( $D_{ZAA}$ , generally at 10-15 m in depth) ranged from  $-3.25$   
 213 to  $-0.56^{\circ}\text{C}$ , and measured ALT varied from 1.0 to 3.75 m. The four study areas were  
 214 all found in the zones of discontinuous permafrost, with poor drainage in lowlands and  
 215 intermontane basins or valleys. The soils in the study area are mainly Histosol and  
 216 Gelisols (Soil Survey Staff, 2014). Before fires, vegetation was dominated by the  
 217 Xing'an larch (*Larix gmelinii*) forest, generally with an understory mainly consisting  
 218 of the shrubs *Ledum palustre* and *Vaccinium uliginosum*, with an organic layer of 55-  
 219 60 cm in thickness. After fires, the vegetation of burned over areas became gradually  
 220 dominated by white birch (*Betula platyphylla*) and dwarf bog birch (*Betula fruticosa*  
 221 Pallas), with an organic layer of 20-30 cm in thickness. At severe burned sites in AL,  
 222 GL, and MH, measurements of organic matter thickness were taken 7, 14, and 29 years  
 223 after fires, so it was possible that the organic layer thickness exceeded 20 cm due to the  
 224 re-accumulation of organic matter. At severe burned site in MG, the organic matter  
 225 residue after combustion was in a fluffy state with the thickness of 20 cm. When the re-  
 226 accumulation or residual organic matter exceeded 20 cm, this would slow the rate of  
 227 active layer thickening and soil temperature increase after fires, as well as the  
 228 permafrost would gradually recover with the re-accumulation of organic layer.

229 Table 1. Characteristics of the eight study sites for monitoring the thermal state and soil nutrients  
 230 of the active layer and near-surface permafrost in the northern Da Xing'anling Mountains in

231 Northeast China

Study areas and sites	Lat	Long.	Elev.	Veget	Organic	Drainage	Fire
-----------------------	-----	-------	-------	-------	---------	----------	------

		(°N)	(°E)	(m a. s. l.)	-ation	layer thickness (cm)		severity
MG	MG-S	52.27	122.28	710	Larch forest	20	Somewhat poor	Severely burned
(Mangui)	MG-U	65	91			55	Poor	Unburned
AL	AL-S	51.88	121.90	669	Larch forest	25	Moderately good	Severely burned
(Alongshan)	AL-U	68	67			55	Poor	Unburned
GL	GL-S	53.04	122.05	582	Shrub wetland	30	Somewhat poor	Severely burned
(Gulian)	GL-U	32	04			60	Poor	Unburned
MH	MH-S	52.98	122.11	486	Shrub wetland	30	Somewhat poor	Severely burned
(Mo'he)	MH-U	59	15			60	Poor	Unburned

232 The horizontal distance between MG-U and MG-S was about 200 m, with the MG-  
 233 U on the edge of the burned area. Observations of ground temperatures began in  
 234 February 2017 (two years after fire). At MG-U in the Xing'an larch (*Larix gmelinii*)  
 235 dominated forest, all larch trees at MG-S were burned to death, and low shrubs and  
 236 herbs were found in 2022. The horizontal distance between AL-U and AL-S was less  
 237 than 100 m, with the AL-U on the edge of the burned area. Observations of ground  
 238 temperatures began in February 2017 (eight years after fire). The vegetation was the  
 239 Xing'an larch forest at AL-U, and; it was the broad-leaved forest (birch) at AL-S. We  
 240 selected GL-S and GL-U sites about 2 km apart from each other. Measurements of  
 241 ground temperatures began in February 2017 (15 years after fire). The vegetation was  
 242 the shrub wetland at GL-U and GL-S. MH-S and MH-U sites were about 5 km apart.  
 243 Observations of ground temperatures began in February 2017 (30 years after fire). The  
 244 ecosystem was characteristic of shrub wetlands at MH-U and MH-S.

## 245 2.2 Fire severity

246 Normalized Burn Ratio (NBR) and differential Normalized Burn Ratio (dNBR)  
 247 are often used to assess the forest fire severity (Cocke et al., 2005; Li et al., 2022b), and

248 the calculation formulas are as follows:

$$249 \quad NBR = (\rho_{NIR} - \rho_{MIR}) / (\rho_{NIR} + \rho_{MIR}) \quad (1)$$

$$250 \quad dNBR = NBR_{prefire} - NBR_{postfire} \quad (2)$$

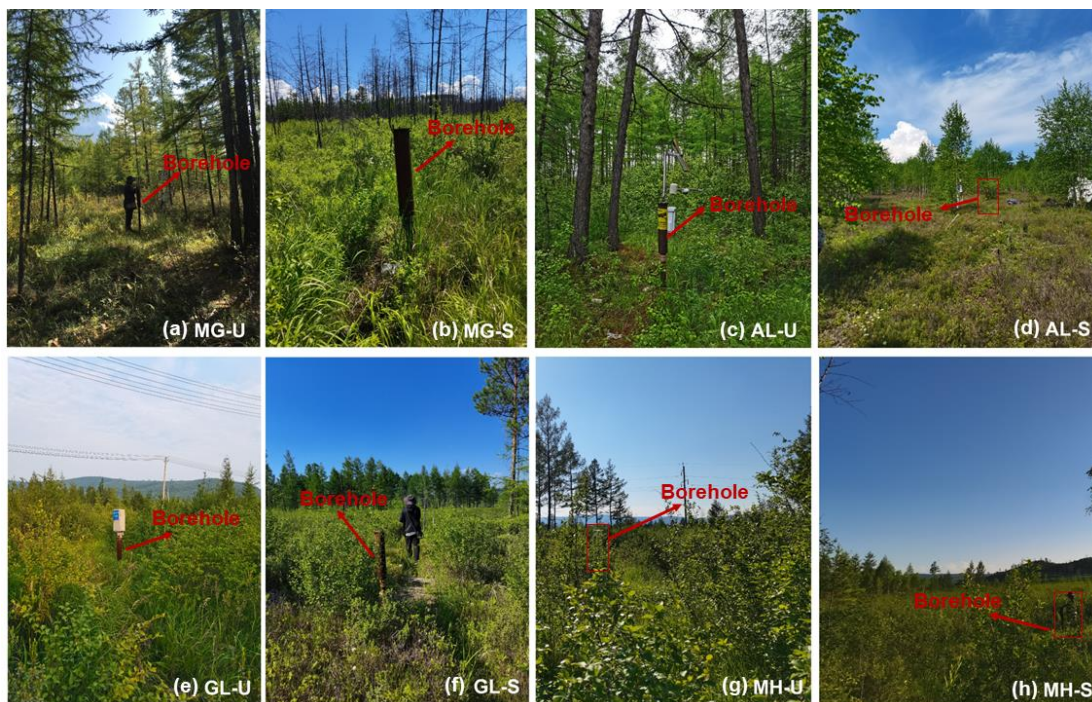
251 where  $\rho_{NIR}$  and  $\rho_{MIR}$  are the reflectivity values of pixel from the near-infrared (NIR)  
252 and middle-infrared (MIR) bands, and;  $NBR_{prefire}$  and  $NBR_{postfire}$  are the values  
253 of NBR before and after fire.

254 According to the Cocke et al. (2005) and Roy et al. (2006), the  $dNBR$  values of  
255 0.241 and 0.57 are the critical values for the division between lightly and moderately  
256 burned, and moderately and severely burned. Therefore, through vegetation burn status  
257 and the comparison with  $dNBR$  values (Key and Benson, 2006; Escuin et al., 2008), fire  
258 severity is thus divided into four categories: severely burned ( $dNBR \geq 0.571$ ),  
259 moderately burned (0.241-0.570), lightly burned (0.051-0.240), and unburned ( $\leq 0.050$ )  
260 (Cocke et al., 2005). In the lightly and moderately burned areas, there were difficulties  
261 in drilling and/or monitoring due to device malfunction or damage. In addition, the  
262 permafrost environment changes more significantly after severe burns. Therefore, only  
263 sites of two levels of fire severity (severely burned and unburned) were chosen for the  
264 abovementioned four areas (Mangui/MG, Alongshan/AL, Gulian/GL and Mo'he/MH)  
265 to study post-fire changes in ground hydrothermal regimes and soil nutrients.

### 266 **2.3 Site instrumentation and laboratory analysis**

267 At each site of unburned and severe burned, a 20-m-deep borehole was drilled and  
268 instrumented in October 2016 to monitor ground temperatures (eight boreholes in total)  
269 (Figure 2). Ground temperatures were monitored with 0.5-m depth intervals at depths  
270 of 0–5 m and then with 1-m depth intervals at depths of 5-20 m by thermistor cables  
271 permanently installed in boreholes and manually measured from February 2017. All  
272 thermistors were assembled and calibrated at the Key Laboratory of Cryospheric  
273 Science and Frozen Soil Engineering, Northwest Institute of Eco-Environment and  
274 Resources (renamed from the merger of the former State Key Laboratory of Frozen Soil  
275 Engineering and the State Key Laboratory of Cryosphere Science, Cold and Arid

276 Regions Environmental and Engineering Research Institute), Chinese Academy of  
 277 Sciences. Since February 2017, ground temperatures at these boreholes were manually  
 278 measured thrice monthly (Table 2), or occasionally once or twice monthly due to traffic  
 279 difficulty or control, by a multi-meter Fluke 189<sup>®</sup> device. According to the measured  
 280 soil temperatures during the observation period, the isotherms of soil temperature in the  
 281 vertical profile at depths of 0-20 m were drawn, and then the 0°C isotherms were  
 282 delineated for each borehole. The values of ALT were then determined, using linear  
 283 extrapolation of seasonally and progressively changing ground temperature distribution  
 284 with depth, for each borehole and each year according to the deepest position of the 0°C  
 285 isotherms in the year.



286  
 287 Figure 2. Photos of the study sites with different vegetation cover and the position of the 20 m deep  
 288 boreholes for monitoring the ground temperature in the northern Da Xing'anling Mountains in  
 289 Northeast China in 3-5 July 2022.

290 Notes: Figures 2a and 2b were the borehole for observation of ground temperature at Xing'an larch  
 291 forest severe burned and light burned sites in MG; Figures 2c and 2d were the borehole for  
 292 observation of ground temperature in a Xing'an larch forest at severe burned and light burned sites  
 293 in AL; Figures 2e and 2f were the borehole for observation of ground temperature in shrub wetlands  
 294 at severe burned and light burned sites in GL; Figures 2g and 2h were the borehole for observation  
 295 of ground temperature at shrub wetlands severe burned and light burned sites in MH.

296 Table 2. Monitoring data for the eight sites of soil nutrients and ground temperature boreholes for studying fire impacts on the permafrost environment in the northern  
 297 Da Xing'anling Mountains in Northeast China

Study sites	Monitoring depths (m)			Time period	Monitoring frequency
	Soil nutrients	Soil gravimetric moisture content (SMC)	Ground temperature		
MG-U	0.1, 0.2, 0.3, 0.4, 0.5, 0.6, 0.7, 0.8, 0.9, 1.0, 1.1, 1.2, 1.3, 1.4, 1.5, 1.6, 1.7, 1.8, 1.9, 2.0, 2.1, 2.2, 2.3, 2.4, 2.5	0.2, 0.3, 0.4, 0.5, 0.6, 0.7, 0.8, 0.9, 1.0, 1.1, 1.2, 1.3, 1.4, 1.5, 1.6, 1.7, 2.0, 2.5, 2.7	0.0, 0.2, 0.5, 1.0, 1.5, 2.0, 2.5, 3.0, 3.5, 4.0, 5.0, 6.0, 7.0, 8.0, 9.0, 10.0, 11, 12, 13, 14, 15, 16, 17, 18, 19, 20	2016; 2016; 2017-2022	Once; Once; Thrice/ month
MG-S	0.1, 0.2, 0.3, 0.4, 0.5, 0.6, 0.7, 0.8, 0.9, 1.0, 1.1, 1.2, 1.3, 1.4, 1.5, 1.6, 1.7, 1.8, 1.9, 2.0, 2.1, 2.2, 2.3, 2.4, 2.5, 2.6	0.2, 0.3, 0.4, 0.5, 0.6, 0.7, 0.8, 0.9, 1.0, 1.1, 1.2, 1.3, 1.4, 1.5, 1.6, 1.7, 1.8, 1.9, 2.0, 2.1, 2.2, 2.6, 4.6, 5.6, 6.1, 7.6	0.0, 0.2, 0.5, 1.0, 1.5, 2.0, 2.5, 3.0, 3.5, 4.0, 5.0, 6.0, 7.0, 8.0, 9.0, 10.0, 11, 12, 13, 14, 15, 16, 17, 18, 19, 20	2016; 2016; 2017-2022	Once; Once; Thrice/ month
AL-U	0.1, 0.2, 0.3, 0.4, 0.5, 0.6, 0.7, 0.8, 0.9, 1.0, 1.1, 1.2, 1.3, 1.4, 1.5, 1.6, 1.7, 1.8, 1.9, 2.0, 2.1, 2.2, 2.3, 2.4, 2.5, 2.6, 2.7, 2.8, 2.9, 3.0	0.1, 0.2, 0.3, 0.4, 0.5, 0.6, 0.7, 0.8, 0.9, 1.0, 1.1, 1.2, 1.3, 1.4, 1.5, 1.6, 1.7, 1.8, 1.9, 2.0, 2.1, 2.2, 2.3, 2.4, 2.5, 2.6, 2.7, 2.8, 2.9, 3.0, 3.1, 3.2, 3.5, 4.0, 4.5, 5.0, 5.5, 5.9, 6.4, 9.4	0.0, 0.2, 0.5, 1.0, 1.5, 2.0, 2.5, 3.0, 3.5, 4.0, 5.0, 6.0, 7.0, 8.0, 9.0, 10.0, 11, 12, 13, 14, 15, 16, 17, 18, 19, 20	2016; 2016; 2017-2022	Once; Once; Thrice/ month
AL-S	0.1, 0.2, 0.3, 0.4, 0.5, 0.6, 0.7, 0.8, 0.9, 1.0, 1.1, 1.2, 1.3, 1.4, 2.1, 2.2, 2.3, 2.4, 2.5, 2.6, 2.7, 2.8	0.2, 0.3, 0.4, 0.5, 0.6, 0.7, 0.8, 0.9, 1.1, 1.4, 1.5, 1.7, 2.0, 2.2, 2.4, 2.6, 2.8, 2.9, 3.1, 3.4, 3.6, 4.0, 4.1, 4.5, 4.8, 5.5, 6.0, 7.0, 7.5	0.0, 0.2, 0.5, 1.0, 1.5, 2.0, 2.5, 3.0, 3.5, 4.0, 5.0, 6.0, 7.0, 8.0, 9.0, 10.0, 11, 12, 13, 14, 15, 16, 17, 18, 19, 20	2016; 2016; 2017-2022	Once; Once; Thrice/ month
GL-U	0.1, 0.2, 0.3, 0.4, 0.5, 0.6, 0.7, 0.8, 0.9, 1.0, 1.1, 1.4, 1.5, 1.6, 1.7, 1.8, 1.9, 2.0, 2.1, 2.2, 2.3, 2.4, 2.5, 2.6, 2.7, 2.8, 2.9, 3.0, 3.1, 3.4, 3.5, 3.6	0.1, 0.2, 0.3, 0.4, 0.5, 0.6, 0.7, 0.8, 0.9, 1.0, 1.1, 1.3, 1.4, 1.5, 1.6, 1.7, 1.8, 1.9, 2.0, 2.7, 2.8, 2.9, 3.0, 3.1	0.0, 0.2, 0.5, 1.0, 1.5, 2.0, 2.5, 3.0, 3.5, 4.0, 5.0, 6.0, 7.0, 8.0, 9.0, 10.0, 11, 12, 13, 14, 15, 16, 17, 18, 19, 20	2016; 2016; 2017-2022	Once; Once; Thrice/ month
GL-S	0.1, 0.2, 0.3, 0.4, 0.5, 0.6, 0.7, 0.8, 0.9, 1.0, 1.2, 1.3, 1.4, 1.5, 2.0, 2.1, 2.2, 2.4, 2.5, 2.6, 2.7, 2.8	0.1, 0.2, 0.3, 0.8, 2.0, 2.4, 2.7, 3.6, 4.2, 4.7, 5.6, 8.4	0.0, 0.2, 0.5, 1.0, 1.5, 2.0, 2.5, 3.0, 3.5, 4.0, 5.0, 6.0, 7.0, 8.0, 9.0, 10.0, 11, 12, 13, 14, 15, 16, 17, 18, 19, 20	2016; 2016; 2017-2022	Once; Once; Thrice/ month
MH-U	0.1, 0.2, 0.3, 0.4, 0.5, 0.6, 0.7, 0.8, 0.9, 1.0, 1.1, 1.4, 1.5, 1.6, 1.7, 1.8, 1.9, 2.0, 2.1, 2.2, 2.3, 2.4, 2.5, 2.6, 2.7, 2.8, 2.9, 3.0, 3.1, 3.4, 3.5, 3.6	0.1, 0.2, 0.3, 0.4, 0.5, 0.6, 0.7, 0.8, 0.9, 1.0, 1.1, 1.3, 1.4, 1.5, 1.6, 1.7, 1.8, 1.9, 2.0, 2.7, 2.8, 2.9, 3.0, 3.1	0.0, 0.2, 0.5, 1.0, 1.5, 2.0, 2.5, 3.0, 3.5, 4.0, 5.0, 6.0, 7.0, 8.0, 9.0, 10.0, 11, 12, 13, 14, 15, 16, 17, 18, 19, 20	2016; 2016; 2017-2022	Once; Once; Thrice/ month
MH-S	0.1, 0.2, 0.3, 0.4, 0.5, 0.6, 0.7, 0.8, 0.9, 1.0, 1.1, 1.2, 1.3, 1.4, 1.5, 1.6, 1.7, 1.8, 1.9, 2.0	0.1, 0.2, 0.3, 0.4, 0.5, 0.6, 0.7, 0.8, 0.9, 1.0, 1.1, 1.2, 1.3, 1.4, 1.5, 1.6, 1.7, 1.8, 1.9, 2.0, 2.3, 3.6	0.0, 0.2, 0.5, 1.0, 1.5, 2.0, 2.5, 3.0, 3.5, 4.0, 5.0, 6.0, 7.0, 8.0, 9.0, 10.0, 11, 12, 13, 14, 15, 16, 17, 18, 19, 20	2016; 2016; 2017-2022	Once; Once; Thrice/ month

298 Notes: Soil nutrients and SMC were observed once in 2016, and soil temperatures were observed thrice monthly in 2017-2022.

299 While drilling in 2016, soil samples were collected from depths of 0-9.4 m at  
300 intervals of 0.1-3.0 m, with a total of 402 soil samples. Three replicas were collected at  
301 the same depth and then three samples were evenly mixed into one. At depths of 0-3.0  
302 m, samples were collected every 10 cm in depth in soil strata with more significant  
303 changes of soil organic matter and lithology near the ground surface. At depths of 3.0-  
304 9.4 m, samples were collected based on lithological similarity or changes in soil or rock  
305 strata, rather than at an equal depth interval of 0.1 m. Therefore, at depths of 0-3 m,  
306 there were generally a set of data at a regular depth interval of 10 cm, but at depths of  
307 3-10 m, the depth intervals of datasets varied substantially. One part of the soil samples  
308 was collected using a cutting ring and stored in an 100-cm<sup>3</sup> aluminum specimen box  
309 and immediately weighed (soil wet weight). Then, the samples were transported to the  
310 laboratory and dried at 105°C to obtain soil dry weight. Finally, gravimetrically-based  
311 SMC was calculated by the mass of soil before and after drying. The other part of the  
312 soil samples was collected and stored in zip-lock bags and timely brought back to the  
313 laboratory for air-drying, then passed through a 2-mm sieve for chemical analysis. SOC  
314 and TN contents were measured by potassium dichromate oxidation reduction and  
315 Kjeldahl nitrate boiling fluid injection methods, respectively (Nelson et al., 1982). TP  
316 and TK contents were determined by the methods of Mo-Sb colorimetry and flame  
317 photometry, respectively (Sun et al., 2011). These data are shown as mean ± standard  
318 error (SE). Changes in ground temperatures and soil chemical properties were analyzed  
319 using the space-for-time chronosequence approach (Mack et al., 2021).

## 320 **2.4 Data quality check**

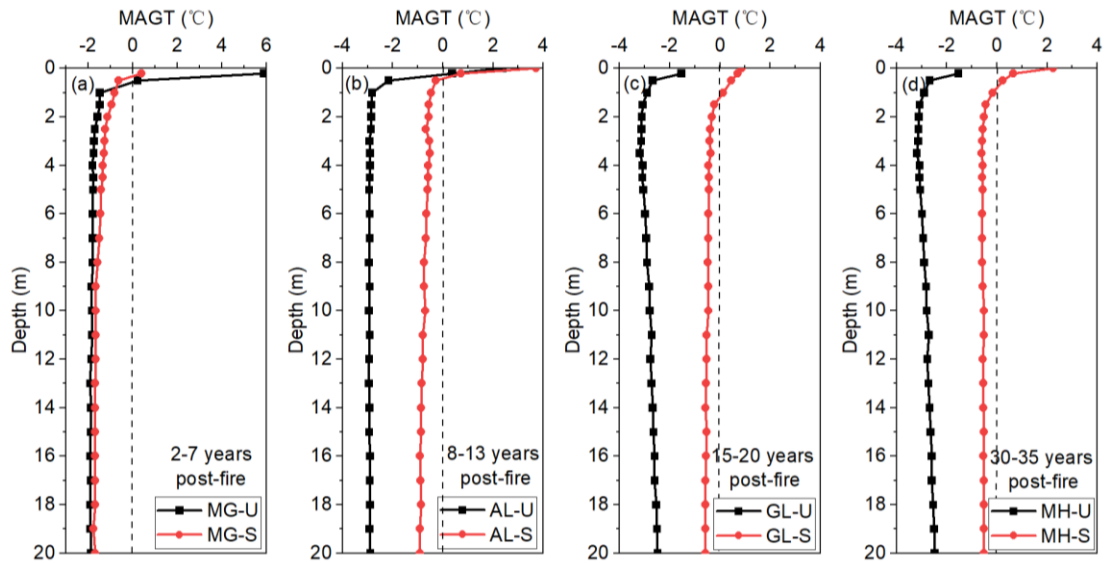
321 The measurement accuracy of ground temperature was ±0.05°C in the range of  
322 -30 to +30°C, but ± 0.1°C in those of -45 to -30°C and +30 to +50°C. From 2020 to  
323 2022, due to the breakout and persistence of the COVID-19 pandemic, some data were  
324 not timely collected, affecting the sampling intervals. Ground temperature data were  
325 collected manually thrice monthly since February 2017, and after the outbreak of the  
326 COVID-19 pandemic, the data were recorded once or twice monthly. In addition, some  
327 data were missing because of damaged, broken, or destroyed probes, solar panel

328 batteries, or dataloggers. From 6 February 2017 to 22 November 2022, a total of 28,890  
329 data records were collected, of which 178 NA (not available) data were resulted from  
330 probe damage, thus 28,712 valid data were collected. All the missing data were near  
331 the ground surface, at a soil layer at depths between 0 and 5 cm. At MG-U, AL-U, AL-  
332 S, GL-S, and MH-S, all data were available. Of the 178 NA data, 74 were at MG-S  
333 (from 17 September 2019 to 22 November 2022), 52 at GL-U (from 20 July 2019 to 13  
334 February 2022), and 52 at MH-U (from 20 July 2019 to 13 February 2022) sites. Data  
335 of soil temperatures from manually monitored boreholes were quality-controlled for  
336 each measurement. Some studies have also shown that this method of monitoring  
337 ground temperature using drilling and probes is one of the most accurate, reliable, and  
338 intuitive methods for long-term monitoring of permafrost data (Chang et al., 2022; Li  
339 et al., 2022a, 2024; Zhao et al., 2021). Before the analysis of soil nutrient data and SMC  
340 data, we conducted outlier tests to ensure the accuracy of the data. These tests showed  
341 that all the data have no outliers and the samples are representative. There was a total  
342 of 840 soil nutrient data and 195 SMC data.

### 343 **3 Data descriptions and evaluation**

#### 344 **3.1 Changes in ground temperatures of near-surface permafrost**

345 Ground temperatures at depths of 0-20 m in the active layer and near-surface  
346 permafrost showed remarkable seasonal dynamics (Figures 3 and 4). The amplitudes of  
347 changes in ground temperature decreased exponentially with increasing depth. At  
348 depths of 0-1 m, changes in MAGT at eight sites were larger 1.5-10.2°C than those at  
349 1-20 m (Figures 3a to 3d).

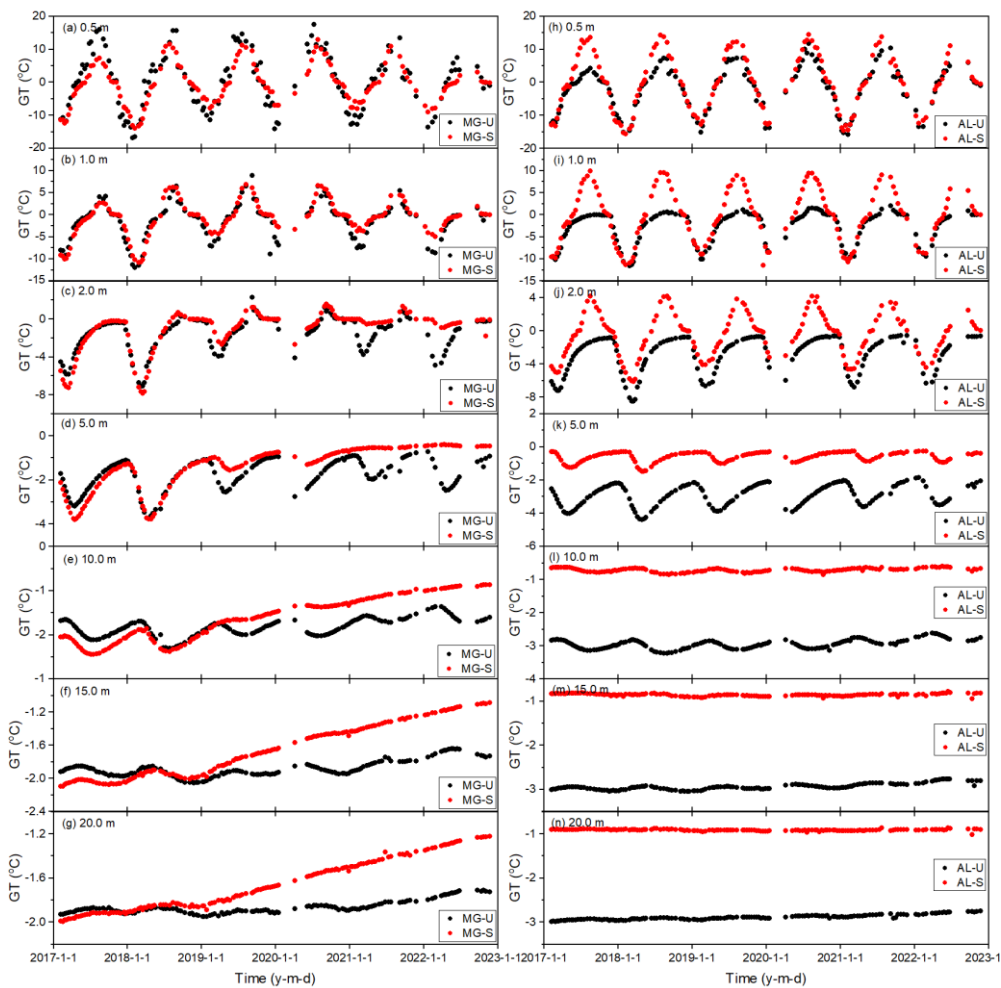


350

351 Figure 3. Mean annual ground temperatures (MAGTs) from 2017 to 2022 at the unburned and

352 severely burned sites in the four areas on the western flank of the northern Da Xing'anling

353 Mountains in Northeast China



354

355 Figure 4. Variability of ground temperatures at depths of 0–20 m at Xing'an larch forest sites in

356 Mangui (MG) and Alongshan (AL) on the western flank of the northern Da Xing'anling Mountains

357 in Northeast China during the period from 2017 to 2022.



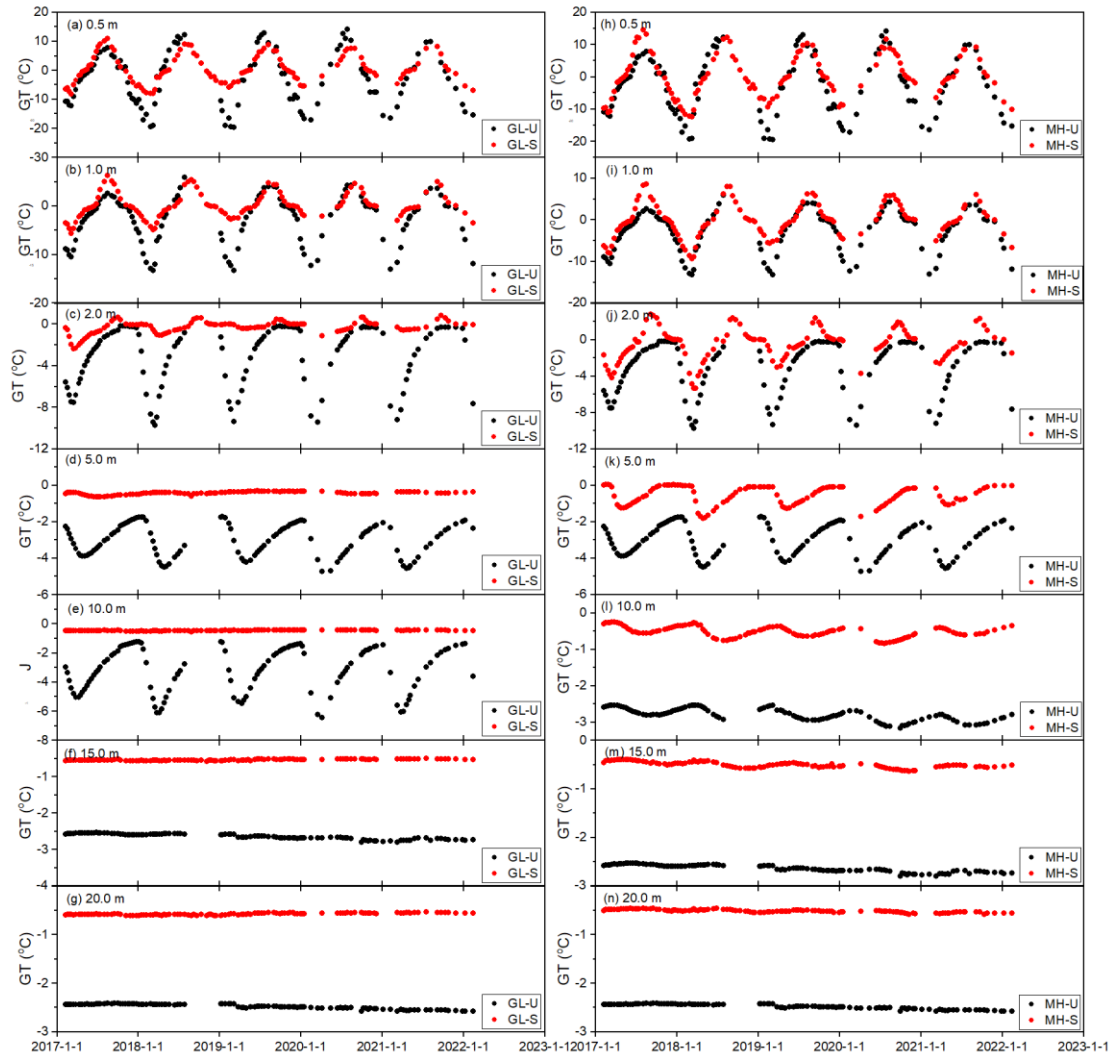
358 Notes: The symbol U stands for the unburned site, S for the severely burned site, and; GT, for ground  
 359 temperature. Figures 4a to 4g were the changes in ground temperatures in Mangui (MG) 2 to 7 years  
 360 after fire; Figures 4h to 4n, those in Alongshan (AL) 8 to 13 years after fire.

361 MAGTs lowered with increasing depths, the temperature difference between 0.5  
 362 and 20 m in depth was 0.2-2.1°C (Table 3). From 2017 to 2022, ground temperature  
 363 fluctuated in a sinusoidal pattern at depths of 0.5 to 2.0 m, and this dynamic change  
 364 gradually disappeared with increasing depth (Figures 3a to 3g and 5a to 5g). At the  
 365 depth of 5 m, ground temperature was subzero or perennially cryotic (Figures 4d, 4k,  
 366 5d, and 5k). At eight sites, from 2017 to 2022, ground temperatures showed an  
 367 increasing trend of 0.01-0.69°C/yr at depths of 0.5-20 m. The increase rate was the  
 368 largest at AL-U (0.03-0.69°C/yr), and; the lowest, at AL-S and GL-S (all were 0.01-  
 369 0.37°C/yr) (Figures 4a to 4g and Figures 5a to 5g).

370 Table 3. Mean annual ground temperatures (MAGTs) at each of the seven measured depths at  
 371 unburned and severely burned sites in the four areas on the western flank of the northern Da  
 372 Xing'anling Mountains in Northeast China during the period from 2017 to 2022

Depth (m)	0.5		1.0		2.0		5.0		10		15		20	
Fire severity	U	S	U	S	U	S	U	S	U	S	U	S	U	S
MG	0.2	-0.6	-1.5	-0.8	-1.6	-1.1	-1.7	-1.4	-1.8	-1.6	-1.9	-1.7	-1.9	-1.7
AL	-2.2	-0.3	-2.8	-0.5	-2.9	-0.6	-2.9	-0.6	-2.9	-0.7	-2.9	-0.9	-2.9	-0.9
GL	-2.7	0.5	-2.9	0.1	-3.1	-0.3	-3.1	-0.4	-2.8	-0.5	-2.6	-0.5	-2.5	-0.6
MH	-2.7	0.2	-2.9	-0.2	-3.1	-0.5	-3.1	-0.6	-2.8	-0.5	-2.6	-0.5	-2.5	-0.5

373 Notes: U stands for unburned sites, and; S, severely burned sites.



374

375 Figure 5. Variations in ground temperatures at depths of 0-20 m at shrub wetlands sites in Gulian  
 376 (GL) and Mo'he (MH) on the western flank of the northern Da Xing'anling Mountains in Northeast  
 377 China during the period from 2017 to 2022.

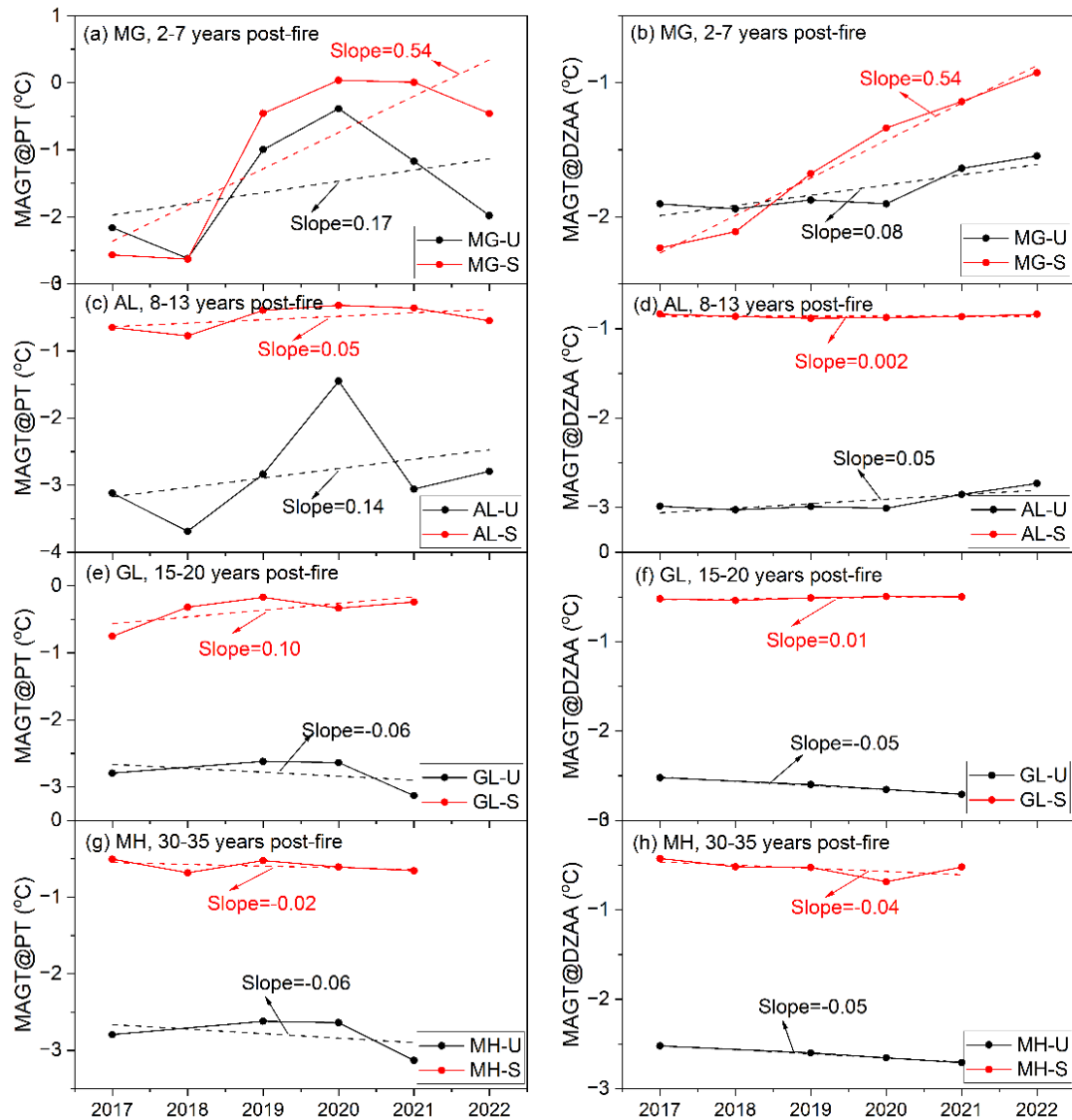
378 Notes: The symbol U stands for the unburned site; S, for the severely burned site, and; GT, for  
 379 ground temperature. Figures 5a to 5g were changes in ground temperatures in GL 15-20 years after  
 380 fire; Figures 5h to 5n, those in MH 30-35 years after fire.

### 381 3.2 Changes in MAGTs at the permafrost table (MAGT<sub>PT</sub>) and D<sub>ZAA</sub> (MAGT<sub>DZAA</sub>)

382 MAGTs at the permafrost table (MAGT<sub>PT</sub>) and at the D<sub>ZAA</sub> (MAGT<sub>DZAA</sub>) can truly  
 383 reflect the changing characteristics of permafrost thermal regimes. Therefore, in this  
 384 section, we have chosen MAGT<sub>PT</sub> and MAGT<sub>DZAA</sub> to briefly analyze changes in ground  
 385 thermal regimes. When the temperature probe was missing at the actual depth of the

386 permafrost table or the  $D_{ZAA}$ ,  $MAGT_{PT}$  and  $MAGT_{DZAA}$  were derived from  
387 interpolation of adjacent ground temperatures.

388 At the eight monitored sites, the burial depths of permafrost table ranged between  
389 1.5 and 4.5 m, and the  $D_{ZAA}$  between 10 and 16 m. From 2017 to 2022, except for GL-  
390 U, MH-U and MH-S sites,  $MAGT_{PT}$  and  $MAGT_{DZAA}$  decreased gradually ( $-0.02$  to  
391  $-0.06^{\circ}\text{C}/\text{yr}$ ), while at other sites increased at rates of  $0.01$ - $0.54^{\circ}\text{C}/\text{yr}$  (Figure 6). The  
392 ground warming rates of  $MAGT_{PT}$  and  $MAGT_{DAZZ}$  were highest at the MG-S site (both  
393 at  $0.54^{\circ}\text{C}/\text{yr}$ ), and lowest at the GL-S site ( $0.10$  and  $0.01^{\circ}\text{C}/\text{yr}$ ) (Figures 6a and 6b).  
394 From 2017-2022, the highest differences in  $MAGT_{PT}$  and  $MAGT_{DAZZ}$  were  $2.6$  and  $1.3^{\circ}\text{C}$   
395 at the MG-S site, respectively, and the lowest were  $0.2$  and  $0.1^{\circ}\text{C}$  at MH-S and AL-S  
396 sites, respectively (Figures 6a, 6d and 6h).



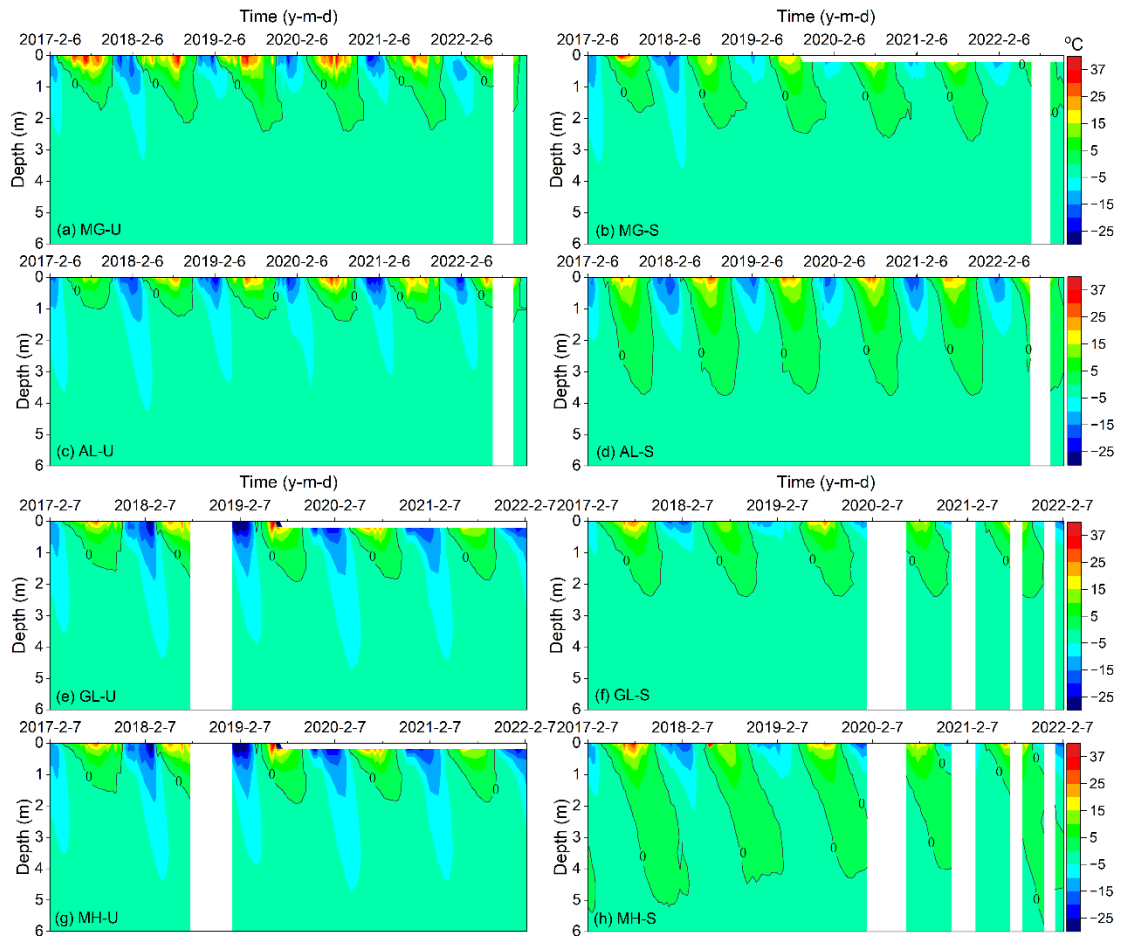
397

398 Figure 6. Variations in mean annual ground temperatures at the permafrost table (MAGT<sub>PT</sub>) and the  
 399 depth of zero annual amplitude (D<sub>ZAA</sub>) (MAGT<sub>DZAA</sub>) at eight sites in the four study areas (Mangui  
 400 or MG, Alongshan or AL, Gulian or GL, and Mo'he or MH) on the western flank of the northern  
 401 Da Xing'anling Mountains in Northeast China during 2017-2022.

402 Notes: U stands for unburned sites, and; S, severely burned sites.

### 403 3.3 Active layer thickness (ALT) data

404 ALT, defined as the annual maximum depth of seasonal thaw penetration, was  
 405 determined according to the deepest position of the 0°C isotherms in a year. Although  
 406 some data were missing, the change trends of ALT were still obvious (Figure 7).

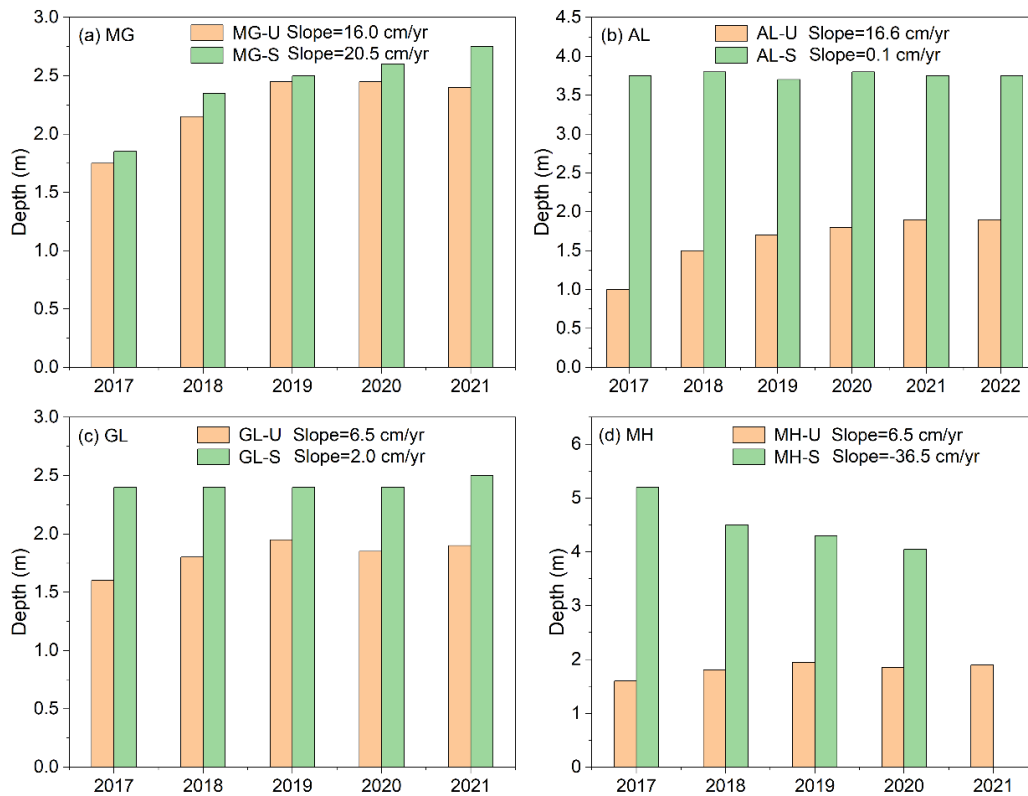


407

408 Figure 7. Variability of ground temperatures isotherms at eight sites in Mangui (MG), Alongshan  
 409 (AL), Gulian (GL), and Mo'he (MH) on the western flank of the northern Da Xing'anling Mountains  
 410 in Northeast China during 2017-2022.

411 Notes: U stands for the unburned sites, as in insets a (site MG-U), c (site AL-U), e (site GL-U), and  
 412 g (site MH-U), and S, the severely burned sites, as in insets b (site MG-S), d (site AL-S), f (site GL-  
 413 S), and h (site MH-S).

414 ALT was between 1.0 and 5.2 m at the eight sites from 2017 to 2022, and the  
 415 maximum average of ALT was 4.5 m at MH-U and the minimum was 1.6 m at AL-U.  
 416 Compared with the other seven sites, MH-S has the largest ALT, with the maximum  
 417 ALT at 5.2 m in 2017. From 2017 and 2022, only at the MH-S site, ALT decreased at a  
 418 rate of 36.5 cm/yr, while at the other sites it increased at rates of 0.1-20.5 cm/yr. The  
 419 increase rate of ALT at MG-S was the fastest, and; at AL-S, the slowest (Figure 8).



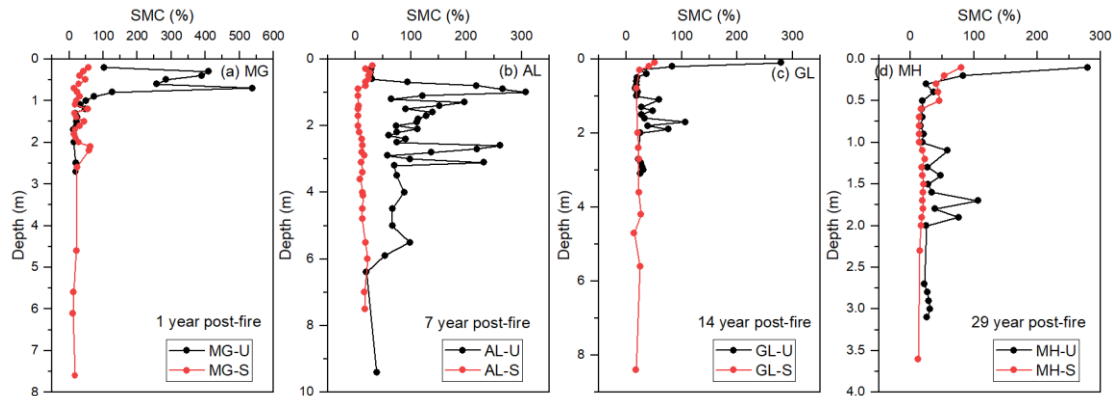
420

421 Figure 8. Variation characteristics of active layer thickness (ALT) from 2017 to 2022 at eight sites  
 422 of the four study areas in Mangui (MG), Alongshan (AL), Gulian (GL), and Mo'he (MH) on the  
 423 western flank of the northern Da Xing'anling Mountains in Northeast China during 2017-2022.  
 424 Notes: U stands for the unburned site, and S, the severely burned site.

### 425 3.4 Variations in gravimetric soil moisture content (SMC)

426 At MG-U and AL-U sites, SMC decreased with increasing depth, especially in the  
 427 active layer and near-surface permafrost, or in the vicinity of the permafrost table  
 428 (Figure 9). For example, at AL-U, SMC decreased at a rate of 8.6%/m and average  
 429 SMC was  $108.2 \pm 11.7\%$  at depths of 0-9.4 m (Figure 9b). At the depths (0-3 m) with  
 430 higher SMC, the soil contains massive ice crystals and a large amount of segregated ice,  
 431 with ice lenses of 0.1–5.0 cm in thickness. For example, at GL-U, SMC was higher at  
 432 the junction of the bottom of the active layer and the upper layer of transient permafrost  
 433 (1-2 m in depth) due to a large amount of segregated ice (0.2-5.0 cm thick) immediately  
 434 under the permafrost table. At MG-S, AL-S, GL-S, and MH-S sites, changes in SMC

435 were inconspicuous, only at depths of 0-0.5 m, with a slight decreasing trend. At depths  
 436 of 0.5-9.4 m, differences in SMC were minor (Figure 9). At MG-S, SMC fluctuated  
 437 between 11.7-63.2% at depths of 0.6-7.6 m, with average SMC at  $27.5\pm 3.2\%$  (Figure  
 438 9a). At AL-S, GL-S, and MH-S sites, SMC fluctuated between 4.7-26.6% at depths of  
 439 0.6-8.4 m, with average SMC of 17.1-21.1%.

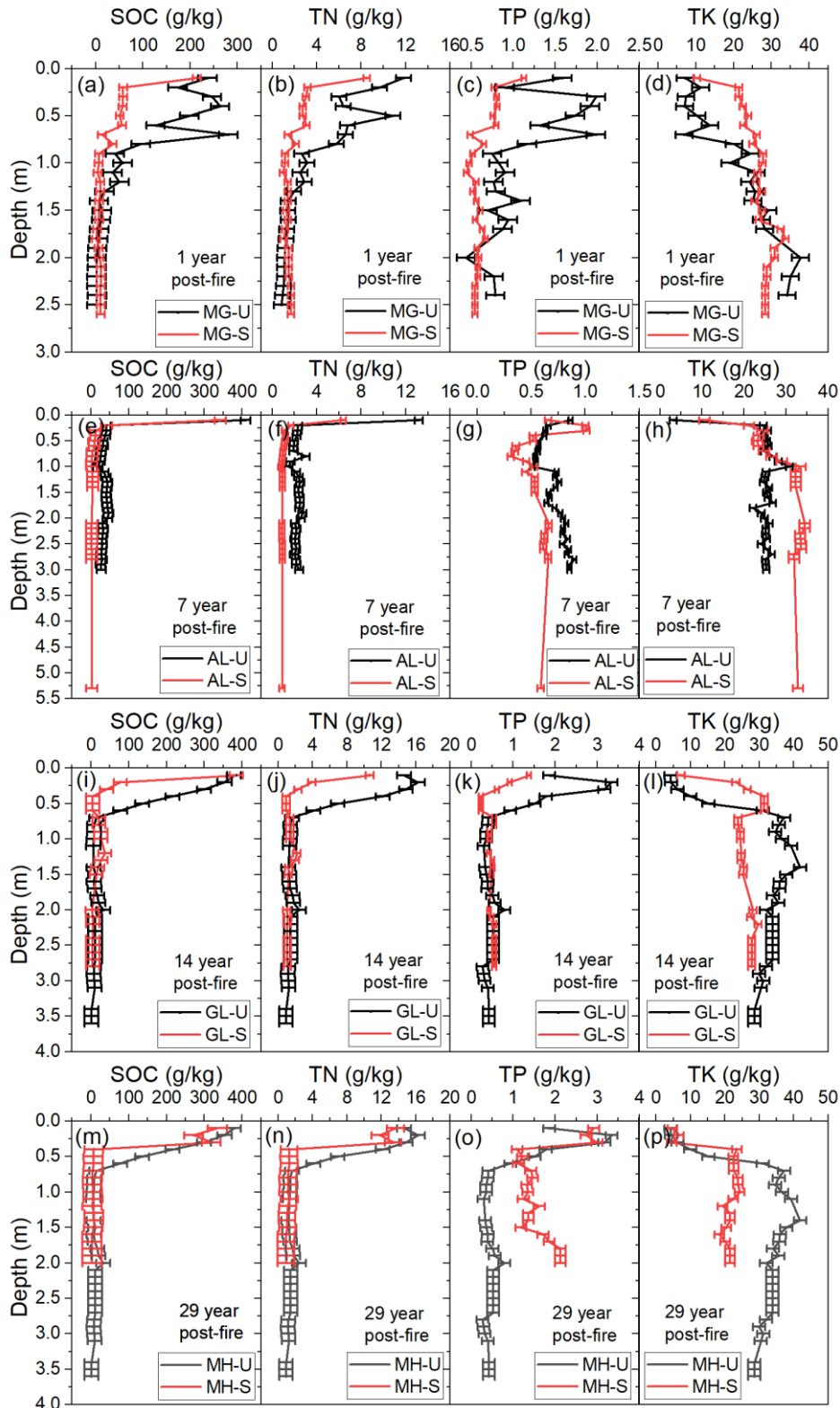


440

441 Figure 9. Variations in gravimetrically-based soil moisture contents (SMC) with different fire severity at eight sites in Mangui (MG), Alongshan (AL), Gulian (GL), and Mo'he (MH) on the  
 442 western flank of the northern Da Xing'anling Mountains in Northeast China in 2016. Notes: The  
 443 symbol U stands for unburned, S for severely burned, and; SMC, for soil gravimetric moisture  
 444 content.  
 445

### 446 3.5 Variations in soil nutrients

447 The contents of SOC and TN decreased with increasing depths. A large amount of  
 448 SOC and TN were stored in the active layer (0-1.3 m), especially in the soil organic  
 449 layer (0-0.5 m) (Figures 10a to 10n). The change trends of SOC and TN were consistent.  
 450 For example, at MG-U, at depths of 0-1.3 m, averages of SOC and TN were  $140.5\pm 26.9$   
 451 and  $5.9\pm 0.9$  g/kg, respectively; at depths of 1.3-2.5 m, changes in SOC and TN were  
 452 relatively smooth, fluctuating between 2.0-13.3 and 0.9-1.5 g/kg, with averages at  
 453  $5.4\pm 1.1$  and  $1.2\pm 0.1$  g/kg, respectively (Figures 10a and 10b).



454

455 Figure 10. Variations in soil nutrients at eight sites in Mangui (MG, a to d), Alongshan (AL, e to  
 456 h), Gulian (GL, i to l), and Mo'he (MH, m to p) on the western flank of the northern Da Xing'anling  
 457 Mountains in Northeast China in 2016.

458 Notes: The symbol U stands for unburned, and S for severely burned. SOC stands for soil organic  
 459 carbon; TN, for total nitrogen; TP, for total phosphorus, and; TK, for total potassium.



460 TP contents decreased up to 1.0 m in depth, and changes in TP were minor at  
461 depths of 1.0-5.3 m (Figures 10c, 10g, 10k, and 10o). For example, at MG-S, TP  
462 decreased at a rate of 0.56 g/kg/m at depths of 0-1.0 m, with an average of  $0.7\pm 0.1$  g/kg  
463 (Figure 10c); TP fluctuated between 0.4 and 0.7 g/kg at depths of 1.1-2.6 m, with an  
464 average of  $0.6\pm 0.01$  g/kg. The change trends of TK were opposite with TP because TK  
465 contents increased downwards (Figures 10d, 10h, 10l, and 10p). The contents of TK  
466 were all below 41.8 g/kg. For example, at MG-U, TK increased at a rate of 14.1 g/kg/m,  
467 while TP decreased at a rate of 0.5 g/kg/m (Figures 10c and 10d).

#### 468 **4. Data availability**

469 The dataset of ground temperature, ALT, SMC, SOC, and contents of TN, TP, and  
470 TK can be freely downloaded and is available from the National Tibetan Plateau/Third  
471 Pole Environment Data Center (<https://doi.org/10.11888/Cryos.tpdc.300933>, Li and Jin,  
472 2024). The dataset was classified into three categories: ground temperatures (at MG-U,  
473 MG-S, AL-U, AL-S, GL-U, GL-S, MH-U, and MH-S), soil moisture contents (SMCs),  
474 and soil nutrient contents (SOC, TN, TP, and TK).

#### 475 **5. Conclusions**

476 The Da Xing'anling (Hinggan) Mountains in Northeast China are located on the  
477 southern margin of the Eastern Asia permafrost zone and boreal forest belt. It is an area  
478 where fires occur frequently and the thermal state of permafrost is sensitive to fire  
479 disturbances. To study fire effects on the permafrost environment, a monitoring network  
480 has been established in Northeast China since 2016. Therefore, a long-term field dataset  
481 on ground hydrothermal regimes and soil nutrients has been obtained. This dataset fills  
482 a gap in a monitoring study of fire effects on the permafrost environment in the  
483 hemiboreal forest zone in Northeast China. These data include ground temperatures at  
484 depths of 0-20 m, SMC at depths of 0-9.4 m, and contents of SOC, TN, TP, and TK at  
485 depths of 0-3.6 m. The data were collected from eight sites in four burned areas (MG  
486 in Mangui, AL in Alongshan, GL in Gulian, and MH in Mo'he) with two categories of  
487 fire severity (severely burned and unburned) from 2016 to 2022.

488 Long-term monitoring data in the northern Da Xing'anling Mountains in Northeast

489 China have shown a degrading permafrost under the disturbances of climate change  
490 and frequent forest fires. This is evidenced by rising ground temperature, thickening  
491 active layer, and evidently changing SMC and soil nutrient contents. The 6-year long  
492 dataset presented in this study has a high-quality time series with only a few missing  
493 data. This valuable and hard-won dataset of forest fires and permafrost is worth  
494 maintaining and improving in the future. This study provides important basic data for  
495 the protection of the ecosystem-dominated Xing'an permafrost and herewith boreal  
496 permafrost ecosystems. Furthermore, it is useful for more accurate prediction of fire-  
497 induced permafrost changes and for more accurate estimating and better-managing soil  
498 carbon stocks. It also provides an important reference for the initiatives of carbon  
499 neutralization and carbon peaking control and the assessment of infrastructure safety  
500 under fire threats.

501 **Author contributions.** XL and HJ designed and conducted this research. XL compiled  
502 the dataset, performed the data analysis, and wrote the manuscript. RH, HW, XC, RŞ, and ZT  
503 participated in the fieldwork. HJ, QF, QW, DL and RŞ improved the writing. XL prepared the  
504 manuscript with contributions from all co-authors.

505 **Competing interests.** The authors declare no conflict of interest.

506 **Disclaimer.** Publisher's note: Copernicus Publications remains neutral with regard to  
507 jurisdictional claims in published maps and institutional affiliations.

508 **Acknowledgments.** We would like to thank all the scientists and students who  
509 participated in the fieldwork. We thank the two anonymous reviewers and editors for  
510 their thorough reviews and insightful comments that improved the paper. We also are  
511 grateful to Professor Xin Li for his encouragement, guidelines, and review of the  
512 proposal for writing up this paper and preparation of the datasets.

513 **Financial support.** This research has been supported by the National Natural  
514 Science Foundation of China (Grant Nos. 42471166 and 32241032); the program of the  
515 Key Laboratory of Cryospheric Science and Frozen Soil Engineering, CAS (Grant No.  
516 CSFSE-ZQ-2407); Heilongjiang Excellent Youth Fund (Grant No. YQ2022D002),

517 National Natural Science Foundation of China (Grant No. 42101408), and;  
518 Fundamental Research Fund for the Central Universities (Grant Nos. 2572023CT01  
519 and 2572021GT08). Raul-David Şerban received funding from the Autonomous  
520 Province of Bozen/Bolzano-Department for Innovation, Research and University  
521 (Grant No. 13585/2023).

## 522 **References**

- 523 Biskaborn, B. K., Smith, S. L., Noetzi, J., Matthes, H., Vieira, G., Streletskiy, D. A., Schoeneich, P.,  
524 Romanovsky, V. E., Lewkowicz, A. G., Abramov, A., Allard, M., Boike, J., Cable, W. L.,  
525 Christiansen, H. H., Delaloye, R., Diekmann, B., Drozdov, D., Eitzelmüller, B., Grosse, G.,  
526 Guglielmin, M., Ingeman-Nielsen, T., Isaksen, K., Ishikawa, M., Johansson, M., Johannsson, H.,  
527 Joo, A., Kaverin, D., Kholodov, A., Konstantinov, P., Kroger, T., Lambiel, C., Lanckman, J. P., Luo,  
528 D., Malkova, G., Meiklejohn, I., Moskalenko, N., Oliva, M., Phillips, M., Ramos, M., Sannel, A. B.  
529 K., Sergeev, D., Seybold, C., Skryabin, P., Vasiliev, A., Wu, Q., Yoshikawa, K., Zheleznyak, M. and  
530 Lantuit, H.: Permafrost is warming at a global scale, *Nat. Commun.*, 10, 264, doi: 10.1038/s41467-  
531 018-08240-4, 2019.
- 532 Boyd, M. A., Walker, X. J., Barnes, J., Celis, G., Goetz, S. J., Johnstone, J. F., Link, N. T., Melvin, A. M.,  
533 Saperstein, L., Schuur, E. A. G. and Mack, M. C.: Decadal impacts of wildfire fuel reduction  
534 treatments on ecosystem characteristics and fire behavior in Alaskan boreal forests, *For. Ecol.*  
535 *Manage.*, 546, 121347, doi: 10.1016/j.foreco.2023.121347, 2023.
- 536 Brown, D. R. N., Jorgenson, M. T., Douglas, T. A., Romanovsky, V. E., Kielland, K., Hiemstra, C.,  
537 Euskirchen, E. S. and Ruess, R. W.: Interactive effects of wildfire and climate on permafrost  
538 degradation in Alaskan lowland forests, *J. Geophys. Res.-Biogeosci.*, 120, 1619-1637, doi:  
539 10.1002/2015jg003033, 2015.
- 540 Certini, G.: Effects of fire on properties of forest soils: A review. *Oecologia*, 143(1), 1–10, 2005.
- 541 Chang, X., Jin, H., Zhang, Y., Li, X., He, R., Li, Y., Lü, L. and Wang, H.: Permafrost thermal dynamics  
542 at a local scale in northern Da Xing'anling Mountains. *Environ. Res. Lett.*, 19(6), 064014. doi:  
543 10.1088/1748-9326/ad42b6, 2024.
- 544 Chang, X., Jin, H., He, R., Zhang, Y., Li, X., Jin, X. and Li, G.: Permafrost changes in the northwestern  
545 Da Xing'anling Mountains, Northeast China, in the past decade, *Earth Syst. Sci. Data*, 14, 3947-  
546 3959, doi: 10.5194/essd-14-3947-2022, 2022.
- 547 Chen, X., Kang, S., Hu, Y. and Yang, J.: Temporal and spatial analysis of vegetation fire activity in the  
548 circum-Arctic during 2001–2020. *Res. Cold Arid Reg.*, 15(1), 48-56,  
549 <https://doi.org/10.1016/j.rcar.2023.03.002>, 2023.
- 550 Chen, Y., Kelly, R., Genet, H., Lara, M. J., Chipman, M. L., McGuire, A. D. and Hu, F. S.: Resilience  
551 and sensitivity of ecosystem carbon stocks to fire-regime change in Alaskan tundra, *Sci. Total*  
552 *Environ.*, 806, 151482, doi: 10.1016/j.scitotenv.2021.151482, 2022.
- 553 Cocke, A. E., Fulé, P. Z. and Crouse, J. E.: Comparison of burn severity assessments using Differenced  
554 Normalized Burn Ratio and ground data, *Int. J. Wildl. Fire*, 14, 189-198, 2005.
- 555 Cunningham, C. X., Williamson, G. J. and Bowman, D. M.: Increasing frequency and intensity of the  
556 most extreme wildfires on Earth. *Nat. Ecol. Evol.*, 1-6, [https://doi.org/10.1038/s41559-024-02452-](https://doi.org/10.1038/s41559-024-02452-2)  
557 [2](https://doi.org/10.1038/s41559-024-02452-2), 2024.

558 Dieleman, C. M., Day, N. J., Holloway, J. E., Baltzer, J., Douglas, T. A. and Turetsky, M. R.: Carbon and  
559 nitrogen cycling dynamics following permafrost thaw in the Northwest Territories, Canada, *Sci.*  
560 *Total Environ.*, 845, 157288, <https://doi.org/10.1016/j.scitotenv.2022.157288>, 2022.

561 Escuin, S., Navarro, R. and Fernandez, P.: Fire severity assessment by using NBR (normalized Burn ratio)  
562 and NDVI (normalized difference vegetation index) derived from Landsat TM/ETM images. *Int. J.*  
563 *Remote Sens.*, 29(4), 1053-1073, 2008.

564 Fultz, L. M., Moore-Kucera, J., Dathe, J., Davinic, M., Perry, G., Wester, D., Schwilk, D. W. and Rideout-  
565 Hanzak, S.: Forest wildfire and grassland prescribed fire effects on soil biogeochemical processes  
566 and microbial communities: Two case studies in the semi-arid Southwest, *Appl. Soil Ecol.*, 99, 118-  
567 128, doi: 10.1016/j.apsoil.2015.10.023, 2016.

568 Genet, H., McGuire, A. D., Barrett, K., Breen, A., Euskirchen, E. S., Johnstone, J. F., Kasischke, E. S.,  
569 Melvin, A. M., Bennett, A., Mack, M. C., Rupp, T. S., Schuur, A. E. G., Turetsky, M. R. and Yuan,  
570 F.: Modeling the effects of fire severity and climate warming on active layer thickness and soil  
571 carbon storage of black spruce forests across the landscape in interior Alaska. *Environ. Res. Lett.*,  
572 8(4), 045016, doi: 10.1088/1748-9326/8/4/045016, 2013.

573 Gu, H., Jin, J., Cheng, X., Wang, E., Zhou, Y. and Chai, Y.: The long-term impacts on chemical properties  
574 of *Larix gmelini* forest on the northern slope of greater Hinggan Mountains from a forest fire of  
575 varying fire intensity (in Chinese). *J Nat Resour*, 25(7), 1114-1121, 2010.

576 Holloway, J. E., Lewkowitz, A. G., Douglas, T. A., Li, X., Turetsky, M. R., Baltzer, J. L. and Jin, H.:  
577 Impact of wildfire on permafrost landscapes: a review of recent advances and future prospects.  
578 *Permafr. Periglac. Process.*, 31(3), 371-382, 2020.

579 Hugelius, G., Strauss, J., Zubrzycki, S., Harden, J.W., Schuur, E.A.G., Ping, C.L., Schirmer, L.,  
580 Grosse, G., Michaelson, G.J., Koven, C.D., O'Donnell, J.A., Elberling, B., Mishra, U., Camill, P.,  
581 Yu, Z., Palmtag, J. and Kuhry, P.: Estimated stocks of circumpolar permafrost carbon with quantified  
582 uncertainty ranges and identified data gaps, *Biogeosciences*, 11, 6573-6593, 2014.

583 Jin, H., Li, S., Cheng, G., Wang, S. and Li, X.: Permafrost and climatic change in China, *Glob. Planet*  
584 *Change*, 26(4), 387-404, doi: 10.1016/S0921-8181(00)00051-5, 2000.

585 Jin, H., Yu, Q., Lü, L., Guo, D., He, R., Yu, S., Sun, G. and Li, Y.: Degradation of permafrost in the  
586 Xing'anling Mountains, northeastern China, *Permafr. Periglac. Process.*, 18(3), 245-258, doi:  
587 10.1002/ppp.589, 2007.

588 Jin, H., Wu, Q. and Romanovsky, V.E.: Editorial: Impacts from degrading permafrost, *Adv. Clim. Change*  
589 *Res.*, 12(1), 1-5. doi: 10.1016/j.accre.2021.01.007, 2021.

590 Jin, H., Huang, Y., Bense, V. F., Ma, Q., Marchenko, S. S., Shepelev, V. V., Hu, Y., Liang, S., Spektor, V.  
591 V., Jin, X., Li, X. and Li X.: Permafrost degradation and its hydrogeological impacts, *Water*, 14(3),  
592 372. doi: 10.3390/w14030372, 2022.

593 Jin, H., Yang, D., Makarieva, O. and Tang, L.: Changes in permafrost and snow cover in the Boreal and  
594 Arctic zones (BAZ) and their impacts, *Adv. Clim. Change Res.*, 14(2), 157-163. doi:  
595 10.1016/j.accre.2023.04.002, 2023.

596 Johnstone, J. F., Chapin Iii, F. S., Foote, J., Kemmett, S., Price, K. and Viereck, L.: Decadal observations  
597 of tree regeneration following fire in boreal forests, *Can. J. For. Res.*, 34(2), 267-273, doi:  
598 10.1139/x03-183, 2004.

599 Johnstone, J. F., Hollingsworth, T. N., Chapin Iii, F. S. and Mack, M. C.: Changes in fire regime break  
600 the legacy lock on successional trajectories in Alaskan boreal forest, *Glob. Change Biol.*, 16(4),  
601 1281-1295, doi: 10.1111/j.1365-2486.2009.02051.x, 2010.

602 Jones, B. M., Grosse, G., Arp, C. D., Miller, E., Liu, L., Hayes, D. J. and Larsen, C. F.: Recent Arctic  
603 tundra fire initiates widespread thermokarst development, *Sci. Rep.*, 5, 15865, doi:  
604 10.1038/srep15865, 2015.

605 Jorgenson, M. T., Harden, J., Kanevskiy, M., O'Donnell, J., Wickland, K., Ewing, S., Manies, K., Zhuang,  
606 Q. L., Shur, Y., Striegl, R. and Koch, J.: Reorganization of vegetation, hydrology and soil carbon  
607 after permafrost degradation across heterogeneous boreal landscapes, *Environ. Res. Lett.*, 8, 035017,  
608 doi: 10.1088/1748-9326/8/3/035017, 2013.

609 Key, C. H. and Benson, N. C.: Landscape assessment (LA). Sampling and analysis methods. D.C. Lutes,  
610 R.E. Keane, J.F. Caratti, C.H. Key, N.C. Benson, S. Sutherland, L.J. Gangi (Eds.), FIREMON: Fire  
611 effects monitoring and inventory system. Integration of standardized field data collection techniques  
612 and sampling design with remote sensing to assess fire effects, U.S. Department of Agriculture,  
613 Forest Service, Rocky Mountain Research Station, Fort Collins, CO, pp. LA1-LA51, 2006.

614 Kirilyanov, A.V., Saurer, M., Siegwolf, R., Knorre, A. A., Prokushkin, A. S., Churakova, O. V., Fonti, M.  
615 V. and Büntgen, U.: Long-term ecological consequences of forest fires in the continuous permafrost  
616 zone of Siberia. *Environ. Res. Lett.*, 15(3), 034061, <https://doi.org/10.1088/1748-9326/ab7469>,  
617 2020.

618 Knicker, H.: How does fire affect the nature and stability of soil organic nitrogen and carbon? A review.  
619 *Biogeochemistry* 85(1), 91–118, 2007.

620 Knorr, W., Arneth, A. and Jiang, L.: Demographic controls of future global fire risk, *Nat. Clim. Change*,  
621 6, 781-785, doi: 10.1038/nclimate2999, 2016.

622 Kolka, R.K., Sturtevant, B.R., Miesel, J.R., Singh, A., Wolter, P.T., Fraver, S., DeSutter, T.M. and  
623 Townsend, P.A.: Emissions of forest floor and mineral soil carbon, nitrogen and mercury pools and  
624 relationships with fire severity for the Pagami Creek Fire in the Boreal Forest of northern Minnesota,  
625 *Int. J. Wildland Fire.*, 26 (4), 296–305, 2017.

626 Kopp, B. J., Minderlein, S. and Menzel, L.: Soil moisture dynamics in a mountainous headwater area in  
627 the discontinuous permafrost zone of northern Mongolia, *Arct. Antarct. Alp. Res.*, 46(2), 459-470.,  
628 2014.

629 Koven, C. D., Schuur, E. A. G., Schädel, C., Bohn, T. J., Burke, E. J., Chen, G., Chen, X., Ciais, P.,  
630 Grosse, G., Harden, J. W., Hayes, D. J., Hugelius, G., Jafarov, E. E., Krinner, G., Kuhry, P.,  
631 Lawrence, D. M., MacDougall, A. H., Marchenko, S. S., McGuire, A. D., Natali, S. M., Nicolsky,  
632 D. J., Olefeldt, D., Peng, S., Romanovsky, V. E., Schaefer, K. M., Strauss, J., Treat, C. C. and  
633 Turetsky, M.: A simplified, data-constrained approach to estimate the permafrost carbon–climate  
634 feedback, *Philos. Trans. R. Soc. Lond. Ser. A-Math. Phys. Eng. Sci.*, 373, 20140423, doi:  
635 10.1098/rsta.2014.0423, 2015.

636 Li, G., Ma, W., Wang, F., Jin, H., Fedorov, A., Chen, D., Wu, G., Cao, Y., Zhou, Y., Mu, Y., Mao, Y.,  
637 Zhang, J., Gao, K., Jin, X., He, R., Li, X. and Li, Y.: A newly integrated ground temperature dataset  
638 of permafrost along the China–Russia crude oil pipeline route in Northeast China, *Earth Syst. Sci.*  
639 *Data*, 14, 5093-5110, doi: 10.5194/essd-14-5093-2022, 2022a.

640 Li, X. and Jin, H.: An integrated dataset of ground hydrothermal regimes and soil nutrients monitored  
641 during 2016-2022 in burned areas in Northeast China. National Tibetan Plateau/Third Pole  
642 Environment Data Center. doi: 10.11888/Cryos.tpdc.300933, 2024.

643 Li, X., Jin, H., He, R., Wang, H., Sun, L., Luo, D., Huang, Y., Li, Y., Chang, X., Wang, L. and Wei, C.:  
644 Impact of wildfire on soil carbon and nitrogen storage and vegetation succession in the Nanweng'he  
645 National Natural Wetlands Reserve, Northeast China, *Catena*, 221, 106797, doi:

646 10.1016/j.catena.2022.106797, 2023.

647 Li, X., Jin, H., He, R., Huang, Y., Wang, H., Luo, D., Jin, X., Lu, L., Wang, L., Li, W., Wei, C., Chang,  
648 X., Yang, S. and Yu, S.: Effects of forest fires on the permafrost environment in the northern Da  
649 Xing'anling (Hinggan) mountains, Northeast China, *Permafr. Periglac. Process.*, 30(3), 163-177,  
650 2019.

651 Li, X., Jin, H., Wang, H., Jin, X., Bense, V. F., Marchenko, S. S., He, R., Huang, Y. and Luo, D.: Effects  
652 of fire history on thermal regimes of permafrost in the northern Da Xing'anling Mountains, NE  
653 China, *Geoderma*, 410, 115670, doi: 10.1016/j.geoderma.2021.115670, 2022b.

654 Li, X., Jin, H., Sun, L., Wang, H., Huang, Y., He, R., Chang, X., Yu, S. and Zang, S.: TTOP-model-based  
655 maps of permafrost distribution in Northeast China for 1961–2020, *Permafr. Periglac. Process.*,  
656 33(1), 425-435, doi: 10.1002/ppp.2157, 2022c.

657 Li, X., Jin, H., Wang, H., Marchenko, S. S., Shan, W., Luo, D., He, R., Spektor, V., Huang, Y., Li, X. and  
658 Jia, N.: Influences of forest fires on the permafrost environment: A review, *Adv. Clim. Change Res.*,  
659 12(1), 48-65, 2021.

660 Liang, L., Zhou, Y., Wang, J. and Gao, X.: Changes of the permafrost environment in Great Xian Ridge  
661 after disastrous forest fire, Taking Gulian mining area as an example (in Chinese), *J. Glaciol.*  
662 *Geocryol.*, 13(1), 17-25, <https://doi.org/10.7522/j.issn.1000-0240.1991.0003>, 1991.

663 Mack, M. C., Bret-Harte, M. S., Hollingsworth, T. N., Jandt, R. R., Schuur, E. A., Shaver, G. R. and  
664 Verbyla, D. L.: Carbon loss from an unprecedented Arctic tundra wildfire, *Nature*, 475, 489-492,  
665 2011.

666 Mack, M. C., Walker, X. J., Johnstone, J. F., Alexander, H. D., Melvin, A. M., Jean, M. and Miller, S. N.:  
667 Carbon loss from boreal forest wildfires offset by increased dominance of deciduous trees, *Science*,  
668 372, 280-283, doi: 10.1126/science.abf3903, 2021.

669 Michaelides, R. J., Schaefer, K., Zebker, H. A., Parsekian, A., Liu, L., Chen, J. Y., Natali, S., Ludwig, S.  
670 and Schaefer, S. R.: Inference of the impact of wildfire on permafrost and active layer thickness in  
671 a discontinuous permafrost region using the remotely sensed active layer thickness (ReSALT)  
672 algorithm, *Environ. Res. Lett.*, 14, 035007, //doi: 10.1088/1748-9326/aaf932, 2019.

673 Munkhjargal, M., Yadamsuren, G., Yamkhin, J. and Menzel, L.: The combination of wildfire and  
674 changing climate triggers permafrost degradation in the Khentii Mountains, northern Mongolia.  
675 *Atmosphere*, 11(2), 155, <https://doi.org/10.3390/atmos11020155>, 2020.

676 Neff, J. C., Harden, J. W. and Gleixner, G.: Fire effects on soil organic matter content, composition, and  
677 nutrients in boreal interior Alaska. *Can. J. For. Res.*, 35(9), 2178-2187, 2005.

678 Nelson, D. W., Sommers, L., Page, A. L., Miller, R. H. and Keeney, D. R., Total carbon, organic carbon,  
679 and organic matter. In: Sparks, D. L., Page, A. L., Helmke, P. A. and Loeppert, R. H. eds, *Methods*  
680 *of Soil Analysis, Part 3*, Soil Science Society of America. Madison, WI, USA, pp. 539-552, 1982.

681 Nossov, D. R., Jorgenson, M. T., Kielland, K. and Kanevskiy, M. Z.: Edaphic and microclimatic controls  
682 over permafrost response to fire in interior Alaska, *Environ. Res. Lett.*, 8, 035013, doi:  
683 10.1088/1748-9326/8/3/035013, 2013.

684 O'Donnell, J. A., Harden, J. W., McGuire, A. D., Kanevskiy, M. Z., Jorgenson, M. T. and Xu, X.: The  
685 effect of fire and permafrost interactions on soil carbon accumulation in an upland black spruce  
686 ecosystem of interior Alaska: Implications for post-thaw carbon loss, *Glob. Change Biol.*, 17(3),  
687 1461-1474, 2011a.

688 O'Donnell, J. A., Harden, J. W., McGuire, A. D. and Romanovsky, V. E.: Exploring the sensitivity of soil  
689 carbon dynamics to climate change, fire disturbance and permafrost thaw in a black spruce

ecosystem, *Biogeosciences*, 8(5), 1367-1382, 2011b.

Petrov, M. I., Fedorov, A. N., Konstantinov, P. Y. and Argunov, R. N.: Variability of permafrost and landscape conditions following forest fires in the Central Yakutian Taiga Zone, *Land*, 11, 496, doi: 10.3390/land11040496, 2022.

Ping, C. L., Michaelson, G. J., Kane, E. S., Packee, E. C., Stiles, C. A., Swanson, D. K. and Zaman, N. D.: Carbon stores and biogeochemical properties of soils under black spruce forest, Alaska, *Soil Sci. Soc. Am. J.*, 74, 969-978, doi: 10.2136/sssaj2009.0152, 2010.

Potter, C. and Hugny, C.: Wildfire effects on permafrost and soil moisture in spruce forests of interior Alaska, *J. For. Res.*, 31(2), 553-563, 2020.

Ramm, E., Ambus, P. L., Gschwendtner, S., Liu, C., Schloter, M. and Dannenmann, M.: Fire intensity regulates the short-term postfire response of the microbiome in Arctic tundra soil. *Geoderma*, 438, 116627, <https://doi.org/10.1016/j.geoderma.2023.116627>, 2023.

Rocha, A. V., Loranty, M. M., Higuera, P. E., Mack, M. C., Hu, F., Jones, B. M., Breen, A. L., Rastetter, E. B., Goetz, S. J. and Shaver, G. R.: The footprint of Alaskan tundra fires during the past half-century: implications for surface properties and radiative forcing. *Environ. Res. Lett.*, 7(4), 044039, <https://doi.org/10.1088/1748-9326/7/4/044039>, 2012.

Roy, D. P., Boschetti, L. and Trigg, S. N.: Remote sensing of fire severity: assessing the performance of the normalized burn ratio. *IEEE Geosci. Remote Sens. Lett.*, 3(1), 112-116, 2006.

Şerban, R.D., Şerban, M., He, R., Jin, H., Li, Y., Li, X., Wang, X. and Li, G.: 46-Year (1973-2019) permafrost landscape changes in the Holo Basin, Northeast China using machine learning and object-based classification, *Remote Sens.*, 13, 1910, doi: 10.3390/rs13101910, 2021.

Shur, Y. L. and Jorgenson, M. T.: Patterns of permafrost formation and degradation in relation to climate and ecosystems, *Permafr. Periglac. Process.*, 18(1), 7-19, 2007.

Smith, S. L., O'Neill, H. B., Isaksen, K., Noetzli, J. and Romanovsky, V. E.: The changing thermal state of permafrost, *Nat. Rev. Earth Environ.*, 3, 10-23, 2022.

Smith, S. L., Riseborough, D. W. and Bonnaventure, P. P.: Eighteen year record of forest fire effects on ground thermal regimes and permafrost in the Central Mackenzie Valley, NWT, Canada, *Permafr. Periglac. Process.*, 26(4), 289-303, 2015.

Soil Survey Staff.: *Keys to Soil Taxonomy*, 12th Edition. Natural Resources Conservation Service, United States Department of Agriculture, Washington D.C., 2014.

Sun, L., Zhao, J. and Hu, H.: Effect of moderate fire disturbance on soil physical and chemical properties of *Betula platyphylla-Larix gmelinii* mixed forest (in Chinese), *Sci. Silvae Sinicae*, 47(2), 103-110, 2011.

Taş, N., Prestat, E., McFarland, J. W., Wickland, K. P., Knight, R., Berhe, A. A., Jorgenson, T., Waldrop, M. P. and Jansson, J. K.: Impact of fire on active layer and permafrost microbial communities and metagenomes in an upland Alaskan boreal forest. *ISME J.*, 8(9), 1904-1919, 2014.

Turetsky, M. R., Abbott, B. W., Jones, M. C., Anthony, K. W., Olefeldt, D., Schuur, E. A. G., Koven, C., McGuire, A. D., Grosse, G., Kuhry, P., Hugelius, G., Lawrence, D. M., Gibson, C. and Sannel, A. B. K.: Permafrost collapse is accelerating carbon release, *Nature*, 569, 32-34, 2019.

Viereck, L.A., Werdin-Pfisterer, N.R., Adams, P.C. and Yoshikawa, K.: Effect of wildfire and fireline construction on the annual depth of thaw in a black spruce permafrost forest in interior Alaska: a 36-year record of recovery. In Kane DL and Hinkel KM eds, *Proceedings of the Ninth International Conference on Permafrost*, Fairbanks, Alaska, USA, June 29 to 3 July, Vol. 2, pp. 1845-1850, 2008.

Wang, H., Jin, H., Che, T., Li, X., Dai, L., Qi, Y., Huang, C., He, R., Zhang, J., Yang, R., Luo, D. and Jin,

- 734 X.: Influences of snow cover on the thermal regimes of Xing'an permafrost in Northeast China in  
735 1960s–2010s, *Permafr. Periglac. Process.*, 35(2), 188-201, doi: 10.1002/ppp.2223, 2024.
- 736 Westerling, A. L., Hidalgo, H. G., Cayan, D. R. and Swetnam, T. W.: Warming and earlier spring increase  
737 Western U.S. forest wildfire activity, *Science*, 313, 940-943, doi: 10.1126/science.1128834, 2006.
- 738 Xu, W., Elberling, B. and Ambus, P. L.: Long-term summer warming reduces post-fire carbon dioxide  
739 losses in an arctic heath tundra, *Agric. For. Meteorol.*, 344, 109823, doi:  
740 10.1016/j.agrformet.2023.109823, 2024.
- 741 Yoshikawa, K., Bolton, W. R., Romanovsky, V. E., Fukuda, M. and Hinzman, L. D.: Impacts of wildfire  
742 on the permafrost in the boreal forests of Interior Alaska, *J. Geophys. Res.*, 108, 8148, doi:  
743 10.1029/2001JD000438, 2003.
- 744 Zhao, K., Zhang, W., Zhou, Y. and Yang, Y.: The influence and countermeasure of forest fire on  
745 environment in Da Xing'anling Mountains (in Chinese), Beijing, Science Press, 1994.
- 746 Zhao, L., Zou, D., Hu, G., Wu, T., Du, E., Liu, G., Xiao, Y., Li, R., Pang, Q., Qiao, Y., Wu, X., Sun, Z.,  
747 Xing, Z., Sheng, Y., Zhao, Y., Shi, J., Xie, C., Wang, L., Wang, C. and Cheng, G.: A synthesis dataset  
748 of permafrost thermal state for the Qinghai–Tibet (Xizang) Plateau, China, *Earth Syst. Sci. Data*,  
749 13, 4207-4218, 2021.
- 750 Zhou, Y., Liang, L. and Gu, Z.: Effects of forest fire on hydro-thermal regime of frozen ground, the  
751 northern part of the Da Hinggan Ling (in Chinese), *J. Glaciol. Geocryol.*, 15, 17-26, 1993.